Research in Astronomy and Astrophysics manuscript no.
(LaTeX: output.tex; printed on August 7, 2025; 23:24)

The Fate of Stars Embedded in AGN Disks Is Determined by an Internal Mixing Threshold

Zheng-Hao Xu[1]

Department of Physics, University of California, Santa Barbara, California, USA; *z_xu@ucsb.edu*

Received 20xx month day; accepted 20xx month day

Abstract Stars can form and evolve within gaseous disks around active galactic nuclei (AGN). In the sub-parsec region of disks around $\sim 10^8 M_\odot$ black holes, stars accrete rapidly, reaching $\gtrsim 200\,M_\odot$ and settling into a quasi-steady state in which accretion balances wind-driven mass loss. Within this environment, their ultimate fate depends critically on the radiative-zone diffusion coefficient ($D_{\rm mix}$), which encapsulates various mixing processes and governs chemical transport between surface and core. Using the `MESA` stellar evolution code, we simulate AGN stars across a range of mixing efficiencies. We find a critical threshold floor value $D_{\rm mix,min} \approx 10^{10}\,{\rm cm^2\,s^{-1}}$ that separates two distinct fates: 1. Immortal stars — when mixing is over-efficient ($D_{\rm mix,min} \gtrsim 10^{10}\,{\rm cm^2\,s^{-1}}$), rapid hydrogen replenishment sustains core hydrogen burning, maintains main-sequence equilibrium, rendering the star effectively "immortal". 2. Metamorphic stars — when mixing is merely efficient ($D_{\rm mix,min} < 10^{10}\,{\rm cm^2\,s^{-1}}$), stars exhaust core hydrogen, evolve off-main-sequence, shed mass to $\approx 15\,M_\odot$, and produce super-solar α-abundances consistent with AGN observations. We conclude that maintaining a mixing floor below this threshold is sufficient to avoid immortality, as flux-induced extra mixing can be effectively modeled via constant floor values. Our estimates provide a foundation for future work on disk enrichment and stellar evolution.

Key words: stars: massive — stars: evolution — accretion, accretion disks — galaxies: active — galaxies: abundances

1 INTRODUCTION

Active galactic nucleus (AGN) disks are extreme environments where stars can exist, either by forming directly in the disk's dense gas (Goodman & Tan 2004; Jiang & Goodman 2011) or by being captured into it (Artymowicz et al. 1993; MacLeod & Lin 2020). Conditions in an AGN disk are far more extreme than in typical starforming regions, gas densities can be billions of times higher and temperatures reach 10^3–10^6 K (Sirko & Goodman 2003). These embedded stars could significantly influence the surrounding disk through

their radiation, winds, and chemical yields (Cantiello et al. 2021; Jermyn et al. 2022; Ali-Dib & Lin 2023; Chen & Lin 2024).

For instance, nuclear burning and later explosions in these stars can seed the disk with C, N, O and other α-elements, helping explain the super-solar metallicities observed in quasar broad-line regions (Hamann & Ferland 1999; Hamann et al. 2002; Nagao et al. 2006; Wang et al. 2022; Huang et al. 2023). Once their fuel is spent, these stars may collapse into black holes or neutron stars (Fryer et al. 2025) later pair up and merge within the disk, suggested for some gravitational-wave sources (Tagawa et al. 2020; Graham et al. 2020). Understanding their full life cycle is the first step toward a unified view of disk enrichment, stellar feedback, and compact-object mergers.

However, the fate of stars embedded in AGN disks is not straightforward. The disk supplies a continuous stream of hydrogen-rich gas, which can either sustain core burning or alter the star's subsequent evolution. We therefore distinguish two evolutionary fates: (1) Stars that remain chemically homogeneous and sustain hydrogen burning indefinitely are termed "immortal stars"; (2) whereas those that accumulate helium in the core and gradually leave the main sequence are termed "metamorphic stars." A critical aspect of stellar evolution within AGN disks is the chemical mixing efficiency, parameterized by $D_{\rm mix}$. Previous studies (Cantiello et al. 2021; Dittmann et al. 2021; Jermyn et al. 2022) show that flux-induced extra internal mixing can allow continuous replenishment of hydrogen to the stellar core, leading to "immortal stars." Latest studies (Ali-Dib & Lin 2023; Fryer et al. 2025) show that in the absence of extra mixing, stars evolve towards "metamorphic" evolutionary pathway, characterized by helium accumulation and post-main-sequence evolution. Clarifying the nature and strength of internal mixing in AGN-embedded stars is therefore essential for accurately modeling their feedback on disk composition and for interpreting the chemical abundances observed in AGN environments.

In this Letter we show that the chemical mixing coefficient in the radiative zone ($D_{\rm mix,min}$) sets the fates of stars inside AGN disks. We begin in § 2 with some analytic estimates of the critical value $D_{\rm crit} \simeq 10^{10}$ cm^2 s^{-1} and explain why flux-induced mixing is equivalent to setting $D_{\rm mix,min} \gtrsim D_{\rm crit}$. In § 3, we present a grid of `MESA` models and track the evolution of stellar mass, luminosity, and core H/He. The results in § 4 show stars with $D_{\rm mix,min} < D_{\rm crit}$ exhaust H and shed mass, while those above this value perpetuate on the main sequence. The trend is consistent across the grid. In § 5, we compare these results with earlier work. Based on these results, we suggest that the sub-critical, "metamorphic" path best matches AGN observations. Although rotation may raise $D_{\rm mix}(r)$, it is unlikely to eliminate this threshold.

2 ANALYTIC THRESHOLD FOR INTERNAL MIXING

For an O/B-type massive star, the radiative temperature gradient in the burning core exceeds the adiabatic gradient, so the Schwarzschild criterion predicts a well-mixed convective core, and the overlying radiative envelope (Kippenhahn & Weigert 1994). In realistic stellar interiors, this mixing arises primarily from rotation-induced fluid motions, including Eddington-Sweet circulation, shear instabilities caused by differential rotation, and magnetohydrodynamic (MHD) processes such as the Tayler-Spruit instability. Although these processes are not explicitly modeled here, it is common to apply the parameter $D_{\rm mix(}r{\rm)}$ to encapsulate their combined efficiency in transporting chemical species radially within radiative zones (Heger et al.

2000). Eddington–Sweet flows (Zahn 1992) produce $D_{\rm mix} \sim 10^3$–$10^5\,{\rm cm^2\,s^{-1}}$ on a $\sim 10^7$yr timescale. Differential-rotation shear generates turbulence with $D_{\rm mix} \sim 10^4$–$10^8\,{\rm cm^2\,s^{-1}}$ (Langer et al. 1985; Maeder & Zahn 1998), while the Tayler–Spruit dynamo can boost mixing to $D_{\rm mix} \gtrsim 10^9$–$10^{14}\,{\rm cm^2\,s^{-1}}$ (Spruit 2002) Observationally, modern asteroseismology has confirmed a wide range of internal mixing efficiencies: some massive B-type stars show almost no extra mixing, whereas others require diffusion coefficients up to $D_{\rm mix} \sim 10^6\,{\rm cm^2\,s^{-1}}$, sustained throughout the main sequence (Pedersen et al. 2021). Our 1D MESA runs follow the standard approach of prescribing a floor $D_{\rm mix,min}$ that represents their combine efficiency in the radiative envelope.

2.1 Diffusion Equation and Timescale Estimate

Analytically, 1D-generalized stellar evolution follows the four classic structure equations—continuity, hydrostatic balance, energy generation, and radiative/convective transport; on top of these, the evolution of the local abundance $X_i(r)$ of species i obeys

$$\frac{\partial X_i}{\partial t} = \mathcal{R}_i + \frac{\partial}{\partial r}\left(D_{\rm mix}(r)\frac{\partial X_i}{\partial r}\right) \approx \mathcal{R}_i + D_{\rm mix,min}\,\frac{X_i}{r^2} \tag{1}$$

where $\mathcal{R}_i$ is the nuclear production rate, $D_{\rm mix}(r)$ is the radial diffusivity and $D_{\rm mix,min} = \min_{Rad.\,Env}\{D_{\rm mix}(r)\}$ is its minimum value through the radiative envelope. The fraction of freshly accreted hydrogen that can reach and fuel core burning is set by the minimum diffusion coefficient $D_{\rm mix,min}$ and by $D_{\rm mix}$ at the core–envelope interface; lowest $D_{\rm mix,min}$ layers act as a bottleneck, so the fresh hydrogen stalls in the envelope regardless of higher $D_{\rm mix}$ further out.

To maintain quasi-homogeneous evolution under continuous disk feeding, the mixing time across the radiative envelope,

$$t_{\rm mix} \simeq \frac{\Delta R^2}{D_{\rm mix}}, \tag{2}$$

where ΔR is radial thickness of the radiative envelope. The equation must not exceed the timescale on which fresh fuel is supplied to (or consumed in) the core,

$$t_{\rm fuel} \simeq \frac{M_{\rm core}\,X_{\rm core}}{\dot{M}_{\rm acc}\,X_{\rm surf} + \dot{M}_{\rm nuc}}, \tag{3}$$

$M_{\rm core}$ is the mass involved in hydrogen burning, $X_{\rm core}$ is the hydrogen mass fraction in the core and $X_{\rm surf}$ is hydrogen mass fraction on stellar surface, and $\dot{M}_{\rm nuc}$ the nuclear mass change rate.

A quick estimation by mass–energy equivalence on $\dot{M}_{\rm nuc}$ the nuclear-consumption rate through the nuclear luminosity [1] via

$$\dot{M}_{\rm nuc} \;=\; \frac{L_\star}{f_{\rm nuc}\,c^2}, \tag{4}$$

where the mass–energy conversion efficiency $f_{\rm nuc}$ depends on the dominant fusion chain ($f_{\rm pp/CNO} \simeq 0.007$, $f_{3\alpha} \simeq 7\times10^{-4}$(Kippenhahn & Weigert 1994)). In astronomical units this is:

$$\begin{aligned}\dot{M}_{\rm nuc} &= \left(\frac{L_\odot}{f_{\rm pp/CNO}\,c^2}\right)\left(\frac{L_\star}{L_\odot}\right)\left(\frac{f_{\rm pp/CNO}}{f_{\rm nuc}}\right)\\ &\simeq 9.6\times10^{-12}\left(\frac{L_\star}{L_\odot}\right)\left(\frac{f_{\rm pp/CNO}}{f_{\rm nuc}}\right) M_\odot\,{\rm yr}^{-1}\end{aligned} \tag{5}$$

[1] Throughout this paper, the luminosity $L_\star$ represents only the stellar nuclear luminosity. Contributions from accretion or gas thermal luminosity are explicitly reflected in the Eddington suppression factor λ_0.

Table 1: Main model parameters and references for detailed settings.

Parameter	Adopted value/reference
Standard mixing floors	$10^1, 10^2, 10^3, \cdots, 10^{13}\,\mathrm{cm^2\,s^{-1}}$
Extra mixing	Flux-induced extra mixing. (See eq.8.)
AGN disk density ($\rho_{\rm AGN}$)	$10^{-16}\,\mathrm{g\,cm^{-3}}$
Gas sound speed ($c_{\rm s}$)	$10^6\,\mathrm{cm\,s^{-1}}$
Disk composition (X_d, Y_d, Z_d)	$(0.739, 0.251, 0.01)$ (near-solar)
Accretion model	Bondi–Hoyle, with radiative feedback (Xu et al. 2025, in prep.)
Wind model	luminosity-driven winds (Xu et al. 2025, in prep.)

Note the constant coefficient is based on pp/CNO cycle calculations. Thus a massive star in AGN disk with $L_\star \sim 10^6 L_\odot$ has $\dot{M}_{\rm nuc} \sim 10^{-6} M_\odot \mathrm{yr}^{-1}$. If He burning dominates, i.e. triple-α process dominates, adopting $f_{3\alpha}$ increases $\dot{M}_{\rm nuc}$ by roughly an order of magnitude.

2.2 Critical Mixing Threshold

In the sub-parsec region of AGN disks, stars' mass accretion rate $\dot{M}_{\rm acc} \sim 10^{-4} M_\odot \mathrm{yr}^{-1} \gg \dot{M}_{\rm nuc}$, and the surface and core hydrogen fractions remain within the same order of magnitude during the main sequence. Therefore $t_{\rm fuel} \approx M_{\rm core}/\dot{M}_{\rm acc}$ (Chen et al. 2025). The critical effective mixing condition $t_{\rm mix} \leq t_{\rm fuel}$ requires a minimum mixing coefficient

$$D_{\rm crit} \gtrsim \frac{\Delta R^2\, \dot{M}_{\rm acc}}{M_{\rm core}}. \tag{6}$$

Adopting $\Delta R \simeq 3 \times 10^{11}\,\mathrm{cm}$ for a massive star's radiative shell, $M_{\rm core} \simeq 30\,M_\odot$, and $\dot{M}_{\rm acc} \simeq 10^{-4}\,M_\odot\,\mathrm{yr}^{-1} \approx 3.2 \times 10^{-12} M_\odot\,\mathrm{s}^{-1}$, we obtain

$$D_{\rm crit} \simeq 1.0 \times 10^{10}\ \mathrm{cm^2\,s^{-1}}. \tag{7}$$

This exceeds the 10^8–$10^9\,\mathrm{cm^2\,s^{-1}}$ typical of rotation-induced shear mixing implied by (Prat & Lignières 2014; Maeder & Meynet 2010; Spruit 2002), implying that most AGN-embedded stars will not remain chemically homogeneous once they reach accretion–wind equilibrium and will therefore evolve off the main sequence despite ongoing mass gain.[2]

Equation (7) provides a convenient order-of-magnitude benchmark for population-synthesis or semi-analytic studies of AGN disk stellar populations. Although real stars host a variety of large-scale circulations and magneto-hydrodynamic dynamos, e.g. Spruit–Tayler instabilities, Eddington–Sweet meridional currents (Spruit 2002), our one-dimensional approach encapsulates their net effect via the chosen $D_{\rm mix} \sim D_{\rm mix,min}$, our 1-D models encapsulate their net effect with the imposed floor $D_{\rm mix,min}$. Low $D_{\rm mix,min}$ preserves core–envelope composition gradients, whereas high values promote near-homogeneous profiles.

3 NUMERICAL METHOD AND MIXING PRESCRIPTIONS

The evolution of a massive star embedded within an AGN accretion disk was modeled using the `MESA v22.11.1` stellar-evolution code (Paxton et al. 2011, 2013, 2015, 2018, 2019; Jermyn et al. 2023), with particular emphasis on the impact of internal mixing on stellar lifetime. We parameterized the 3D-MHD simulation results from Chen et al. (2024) into boundary conditions for the stellar atmosphere, modifying them to reflect Bondi-Hoyle accretion and the radiative feedback from the accreting gas. Surface luminosity-driven winds were also included to account for mass loss. Detailed prescriptions for the accretion rate $\dot{M}_{\rm acc}$, radiative feedback $S_{\lambda_0}(L_\star/L_{\rm Edd})$, and wind loss $\dot{M}_{\rm wind}$ are provided in Xu et al. (2025, in preparation).

Main parameters are summarized in Table 1. The main model grid explores a range of chemical mixing prescriptions, including both a constant floor diffusivity and the flux-induced extra mixing scheme. A suppression factor $S_{\lambda_0}(\lambda_\star)$ is applied with $\lambda_0 = 0.75$, i.e. $\lambda_\star \equiv L_\star/L_{\rm Edd} \lesssim \lambda_0$ This factor incorporates the radiative-feedback behaviour extracted from the 3-D simulations of Chen et al. (2024). A comprehensive exploration of this extended parameter space will be presented in Xu et al. (2025, in preparation).

3.1 Standard Mixing Prescriptions

Chemical mixing in 1D models, particularly within the stellar core, follows the standard Mixing-Length Theory (MLT) (Joyce & Tayar 2023), in which the diffusion coefficient is approximated by $D_{\rm mix} \propto 0.33\, v_{\rm conv}\, \alpha_{\rm MLT}$; we keep the default value $\alpha_{\rm MLT} = 2.0$ in `MESA`. In the radiative envelope, the diffusion coefficient for chemical mixing is enforced by setting the flag `set_min_D_mix=.true.` and defining `min_D_mix=<value>` in the `controls` namelist. When `set_min_D_mix` is enabled, `D_mix` in every mesh cell is ensured to be at least `min_D_mix`. This approach provides a straightforward implementation to mimic unresolved physical mixing processes— such as microscopic diffusion, shear turbulence, or weak circulation—in radiatively stable regions without explicit hydrodynamics (Paxton et al. 2018).

To investigate the role of microscopic mixing in radiative zones, we impose a floor diffusion coefficient $D_{\rm mix,min}$ ranging from 10^1 to $10^{13}\,{\rm cm^2\,s^{-1}}$. In practice, this prescription ensures that each mesh cell exchanges material with its neighbor at no less than $D_{\rm mix,min}$, thereby enforcing a minimum rate of chemical diffusion throughout the radiative envelope.

3.2 Flux-Induced Extra Mixing Prescriptions

The immortal stars are constructed with an "extra" mixing prescription, in which $D_{\rm mix,min}$ is assumed to increase with stellar radiation flux F. The form of this additional diffusivity, in Eq. (20) of Cantiello et al. (2021), is set to be the same order as that in the convective region, i.e.

$$D_{\rm extra-mix}(r) \propto \left(\frac{F}{\rho}\right)^{1/3} \tanh(\lambda_\star^7). \tag{8}$$

This expression defines how $D_{\rm mix}(r)$ depends on the Eddington factor $\lambda_* = L_*/L_{\rm Edd}$ where $L_{\rm Edd}$ is the Eddington luminosity. As λ_* increases from 0 to nearly 1, $D_{\rm mix}(r)$ grows exponentially. Hereafter, we denote the flux-induced mixing prescription as 'ExtraMix'.

[2] The value of $D_{\rm crit}$ scales linearly with $\dot{M}_{\rm acc}$ and quadratically with ΔR, so thinner envelopes or lower accretion rates reduce the requirement. A full parameter survey is presented in Xu et al. 2025 in prep.

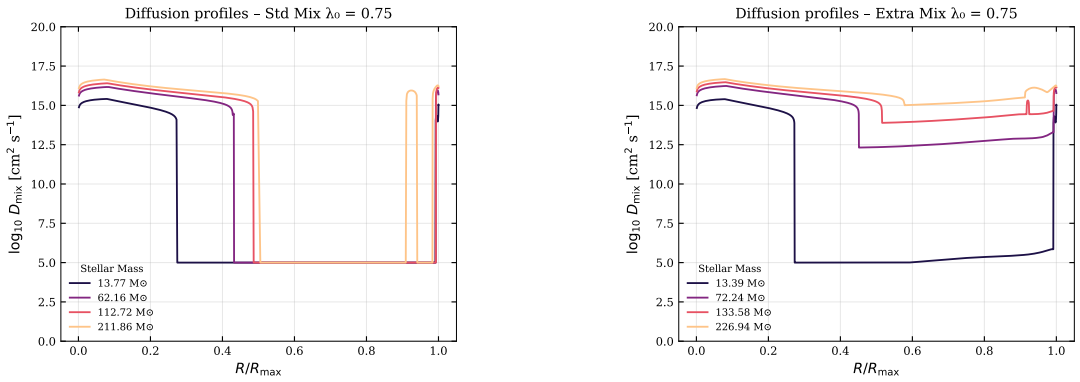

(a) Standard mixing with $D_{\rm mix,min} = 10^5$

(b) Flux-induced extra mixing

Fig. 1: Radial profiles of the chemical-mixing diffusivity $D_{\rm mix}(r)$ used in our models in their main sequence stages from initial to near the quasi accretion-wind equilibrium. (a) Under the standard mixing, the radiative envelope's diffusivity remains fixed at the floor value. The core builds up helium and the star follows the "metamorphic" evolution pathway. (b) With inner radiative flux-induced "extra" mixing prescription, the "immortal" star shows super-critical diffusivity in envelope, continuously replenishes core hydrogen. Here $\lambda_0 = 0.75$ sets the radiative-feedback suppression threshold.

4 RESULTS

We computed a suite of MESA runs in which only the floor diffusion coefficient in radiative zones, $D_{\rm mix\,,\,min}$, is changed. The grid spans $\log_{10}(D_{\rm mix,min}) = 1, 2, \cdots, 13\,{\rm cm^2\,s^{-1}}$ plus one flux-induced "ExtraMix" case that follows the extra-mixing prescription of eq. 8. All other AGN-disk parameters are summarized in Table 1 and are similar to those adopted in Ali-Dib & Lin (2023) and Fryer et al. (2025). We restrict the maximum model time step to $\Delta t < 10^{10}\,{\rm s}$ during phases of rapid mass change, in order to avoid numerical instabilities. The MESA inlists are available at GitHub repository.

4.1 Radial Mixing Profiles

Figure 1 compares the radial mixing-diffusivity profiles of our standard mixing models with flux-induced extra mixing one. We plot four snapshots per model (in different colors), corresponding to increasing stellar mass during the ramp-up phase.

In panel 1a, we show that even with a constant mixing floor of $D_{\rm mix,min} = 10^5, {\rm cm^2\,s^{-1}}$, the radial profile remains broadly similar throughout mass growth. The core boundary gradually moves outward, but the shape and level of the diffusion profile stay roughly constant. We will show later in Table 2 that for $D_{\rm mix,min}$ below the critical threshold, modest variations in the floor value do not significantly affect the overall stellar evolution. Panel **??** shows that under the flux-induced "extra" mixing scheme, the floor value of $D_{\rm mix}$ rises rapidly as the star grows and approaches the Eddington limit. Specifically, $D_{\rm mix,min}$ increases from $\sim 10^5\,{\rm cm^2\,s^{-1}}$ at low mass to $\gtrsim 10^{13}\,{\rm cm^2\,s^{-1}}$ once $M_* \gtrsim 100\,M_\odot$, making both the envelope and core nearly fully convective. The fluctuations near the surface seen in both profiles reflect physical subsurface convective shells, such as those driven by helium or opacity-induced ionization zones.

Table 2: Metamorphic star models for various floor diffusivity $\log_{10}(D_{\rm mix,min}/{\rm cm^2\ s^{-1}})$. Masses are in $M_\odot$, stellar ages t in Myr, and luminosities are $\log(L/L_\odot)$.

$\log_{10}(D_{\rm mix,min})$	1	2	3	4	5	6	7	8	9
$M_{\rm max}$	234.034	234.080	234.057	234.245	233.956	234.376	234.241	234.233	233.860
$t_{\rm max}$	5.390	5.386	5.402	5.405	5.400	5.398	5.403	5.399	5.388
$\log L_{\rm max}$	6.674	6.674	6.674	6.674	6.674	6.674	6.674	6.674	6.673
$M_{\rm TAMS}$	14.816	14.813	14.818	14.808	14.810	14.803	14.704	14.165	13.876
$t_{\rm TAMS}$	8.380	8.380	8.377	8.379	8.376	8.378	8.391	8.501	8.813
$\log L_{\rm TAMS}$	5.374	5.374	5.374	5.375	5.374	5.374	5.371	5.353	5.345

Table 3: Immortal star models at high $\log_{10}(D_{\rm mix,min}/{\rm cm^2\ s^{-1}})$ and for the ExtraMix prescription. Masses are in $M_\odot$, ages t in Myr, and luminosities are $\log(L/L_\odot)$.

$\log_{10}(D_{\rm mix,min})$	10	11	12	13	ExtraMix
$M_{\rm max}$	227.486	224.631	227.706	229.987	230.132
$t_{\rm max}$	5.361	5.368	5.399	5.422	5.413
$\log L_{\rm max}$	6.661	6.656	6.662	6.666	6.667
$M_{\rm eq}$	31.610	143.005	211.123	221.539	221.921
$\log L_{\rm eq}$	5.727	6.451	6.628	6.650	6.650

4.2 Comparative Evolution of Metamorphic and Immortal Stars

Our key finding is a sharp transition at $D_{\rm mix,min} \sim 10^{10}$ cm^{2}s^{-1} (Fig. 2). Below this value: the star cannot keep its core hydrogen-rich. It becomes a "metamorphic star" — builds up helium, leaves the main sequence, and sheds mass (Ali-Dib & Lin 2023; Chen & Lin 2024). Table 2 shows the stellar masses of metamorphic stars at the terminal-age main sequence (TAMS). These stars evolve into intermediate post-main-sequence stars that eventually undergo core collapse, producing black holes or supernovae. As shown in Table 3, above this $D_{\rm mix,min}$ value, the star mixes fast enough to keep burning hydrogen. It does not move off the main sequence, i.e. it has become an "immortal" star. Its mass stays steady, burning hydrogen as fast as gas comes in. However, this case is likely unrealistic. The required mixing is stronger than what rotation or known physics can provide. Also, it would produce too much helium in the disk, which is not seen in AGN spectra (Nagao et al. 2006; Wang et al. 2022; Huang et al. 2023).

The evolution of an AGN star, as shown in Fig. 3, can be divided into three main stages. Initially, the star accretes mass from the disk, with both stellar mass and luminosity increasing steadily while the core hydrogen and helium fractions remain nearly constant. During this phase, the net accretion rate

$$\dot{M}_{\rm net} = \dot{M}_{\rm acc} - \left|\dot{M}_{\rm wind}\right| \tag{9}$$

is typically $\sim 10^{-4} M_\odot {\rm yr}^{-1}$ (see Fig. 4). As the star approaches its maximum mass, the luminosity quickly rises, with $L_*/L_{\rm Edd}$ reaching up to 0.8. At this point, accretion tapers off and the system transitions to a state where further growth is limited by radiative feedback and stellar winds Chen et al. (2024).

For all "metamorphic" runs with $\log_{10} D_{\rm mix,min} < 10\,{\rm cm^2\ s^{-1}}$, the mass–time curves sit almost on top of one another (as shown in table 2), at any epoch their stellar masses differ by $\lesssim 4\%$ (median deviation $<$

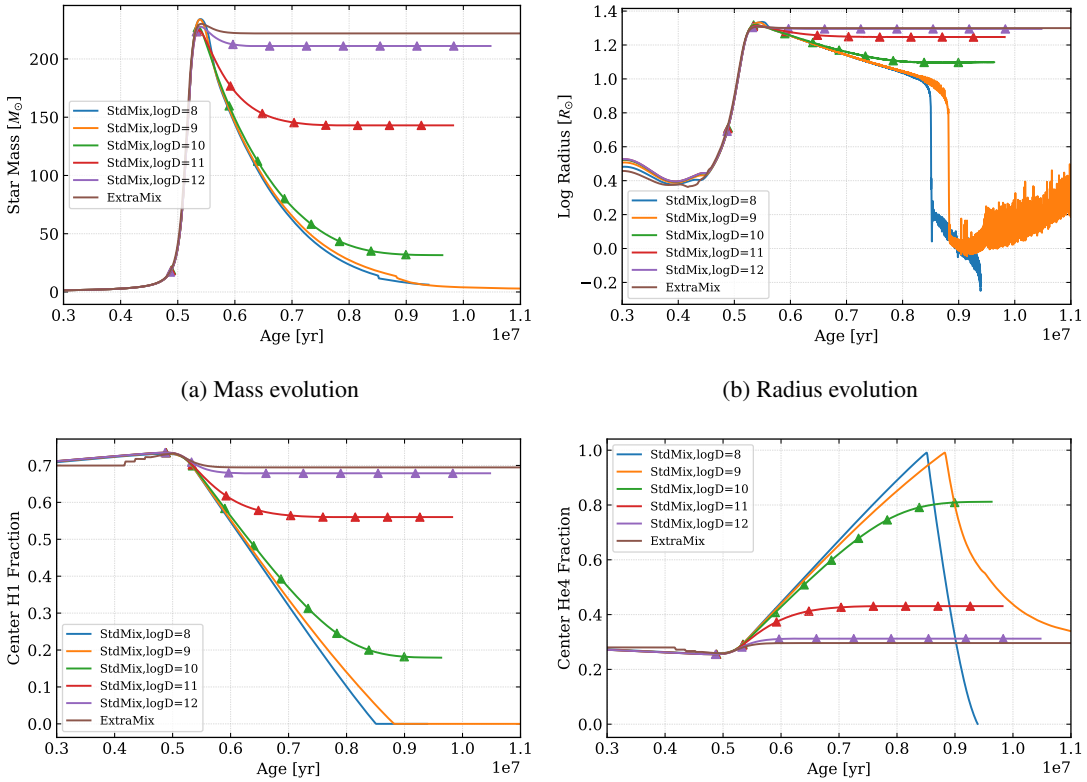

(a) Mass evolution

(b) Radius evolution

(c) Central hydrogen abundance

(d) Central helium abundance

Fig. 2: Evolution of stellar properties for models with different mixing efficiencies. (a) Mass versus age; (b) Radius versus age; (c) Central hydrogen mass fraction versus age; (d) Central helium mass fraction versus age. Models with $D_{\rm mix,min} = 10^8, 10^9, 10^{10}, 10^{11}, 10^{12}$ cm^2 s^{-1} and the flux-induced ExtraMix run are shown. Triangles mark "immortal stars" (continuing H burning). Common inputs: $\rho_{\rm AGN} = 10^{-16}\,{\rm g\,cm^{-3}}$, $c_{\rm s} = 10^6\,{\rm cm\,s^{-1}}$, solar (X, Y, Z); the suppression factor drops to near 0 when $\lambda_\star \geq \lambda_0\, L_{\rm Edd}$, and each $\log D$ sets the floor minimum $D_{\rm mix,min}$.

1%). This confirms that once mixing is below the threshold value (i.e $D_{\rm mix,min} < 10^{10}{\rm cm^2 s^{-1}}$), accretion stops growing at maximum mass (lower left panel (c) in Fig. 3). The supply of fresh hydrogen to the core depends entirely on the magnitude of $D_{\rm mix,min}$. If mixing is weak, helium builds up in the center, increasing the luminosity and enhancing mass loss, which can trigger a runaway mass-loss phase (see also the decline in net accretion rate after the mass peak in Fig 4). As summarized in Table 2, these stars reach a maximum mass near $\sim 230, M_\odot$ but quickly transition off the main sequence as the central hydrogen mass fraction drops below 10^{-4} (panel 2c). The final mass at the terminal-age main sequence (TAMS) is much lower, indicating evolution toward a core-collapse supernova and possibly a luminous envelope outburst (Fryer et al. 2025). Further details on remnant masses are discussed in Xu et al. (2025, in prep.).

By contrast, when $D_{\rm mix,min} \gtrsim 10^{10}{\rm cm^2 s^{-1}}$ or with flux-induced extra mixing, stars reach a quasi-steady equilibrium where the core is efficiently supplied with hydrogen (panel (c) in Fig. 2), and mass-loss and accretion rates balance (see Table 3). These "immortal" stars do not exhaust their core hydrogen and remain on the main sequence indefinitely, provided the disk environment persists. The flux-induced extra mixing ensures that the entire star becomes almost fully convective, so that any newly accreted hydrogen is rapidly transported to the burning core and processed helium is efficiently redistributed. For intermediate

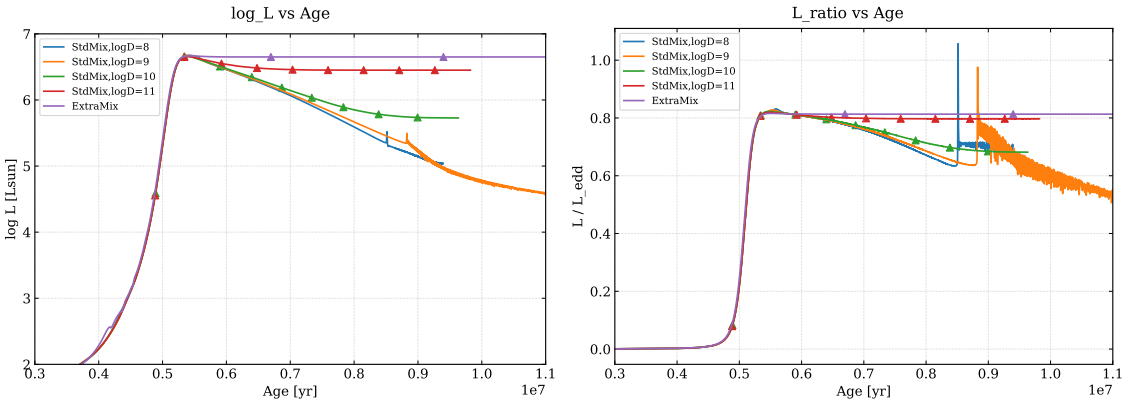

(a) Stellar luminosity $\log L$

(b) Luminosity ratio $L_\star/L_{\rm Edd}$

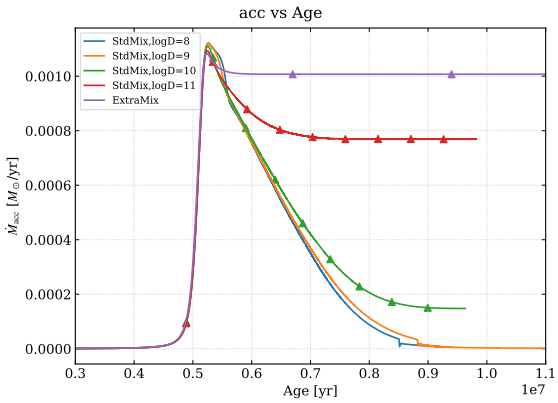

(c) Mass accretion rate $\dot{M}_{\rm acc}$

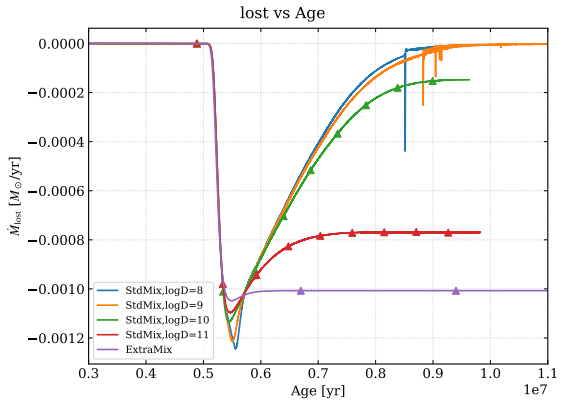

(d) Mass-loss rate $\dot{M}_{\rm lost}$

Fig. 3: Evolutionary tracks for representative models, showing (a) stellar luminosity $\log L_\star$, (b) luminosity relative to Eddington $L_\star/L_{\rm Edd}$, (c) mass accretion rate $\dot{M}_{\rm acc}$, and (d) mass-loss rate $\dot{M}_{\rm lost}$ as functions of stellar age.

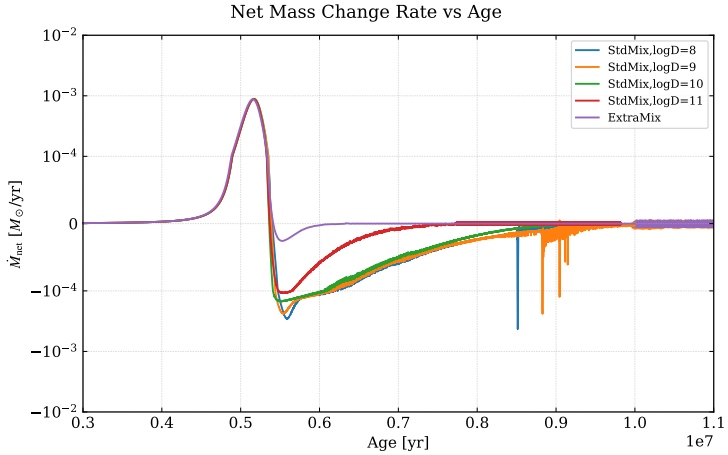

Fig. 4: Net stellar mass-change rate ($\dot{M}_{\rm net} = \dot{M}_{acc} - |\dot{M}_{wind}|$) as a function of time for the same models shown in Fig. 3.

mixing values ($D_{\rm mix,min} \sim 10^{10}{\rm cm}^2\,{\rm s}^{-1}$), we find the central helium fraction increases slowly as equilibrium is established (panel 2d in Fig. 2), but mixing remains strong enough to maintain near steady-state

core hydrogen burning. For low-mixing cases ($D_{\rm mix,min} \leq 10^9 {\rm cm^2 s^{-1}}$), evolutionary tracks are nearly indistinguishable from each other , both the evolution time and final mass change only modestly.

In summary, the results of MESA models confirm the existence of a critical mixing threshold at $D_{\rm mix,min} \sim 10^{10} {\rm cm^2 s^{-1}}$ (see Eq. 7), in agreement with theoretical expectations. Below this threshold, stars evolve as "metamorphic" objects, rapidly exhausting core hydrogen and losing mass; above it, efficient mixing leads to quasi-immortal stars capable of sustained growth and persistent hydrogen burning.

5 DISCUSSION

Luminous AGNs are surrounded by disks with high accretion rate (Yu & Tremaine 2002; Shankar et al. 2009). The disk regions beyond 10^2–10^3 Schwarzschild radii subject to gravitational instability where fragmentation leads to *in situ* star formation (Chen et al. 2023). The dense gas around these stars provides reservoirs of persistent post-formation accretion. Their intrinsic nucleosynthetic luminosity increases with radiative feedback, which reduces the accretion rate and drives a stellar wind. As it approaches the Eddington limit, mass exchange between the embedded massive stars and the disk continues albeit at a reduced rate and with negligible net value(Chen & Lin 2024).

Rotation-driven transport alone is unlikely to raise $D_{\rm mix}$ above our critical bar as well. First, accretion flows in AGN disks are highly time-variable and prone to stochastic angular-momentum flips (Chen & Lin 2023). Second, even when steady rotation is enforced, the ES meridional velocity predicted by 1D MESA prescriptions exceeds the two-dimensional hydrodynamic value by more than an order of magnitude (Mombarg et al. 2024), implying that realistic shear mixing is weaker than often assumed in stellar models. The full impact of stellar rotation will be explored in future work.

The H-rich disk gas enters the star through its surface which is insulated from its nuclear-burning convective core by a radiative layer (Ali-Dib & Lin 2023). Whereas the homogenization of abundance in the convective core can be approximated by a mixing length prescription, that through the radiative envelope is poorly understood. Estimates for the diffusion coefficient through this laminar region ranges from negligible molecular chemical diffusivity to *ad hoc* "extra-mixing" prescription for meridional circulation induced by the intense radiative flux emerging from near-Eddington massive-star cores.

We carry out a series of MESA models to show that extra mixing generally leads to sufficient gas exchange to replenish the H-fuel in the core. In this case, the embedded stars persistently preserve their mass and internal composition, becoming "immortal" stars. However, below a modest threshold ($D_{\rm mix,min} \lesssim 10^{10}$ cm^2 s^{-1}, including the conventional estimates), the He abundance in the stellar core continuously increases at the expense of H depletion until the star evolves onto the post-main-sequence track. Eventually these metamorphic stars undergo core collapse and release both α elements and Fe (Fryer et al. 2025).

The results presented here highlight the importance of elemental mixing efficiency in determining the outcome of stellar evolution. In a follow-up paper (Xu et al. 2025, in prep.), we will carry out extensive studies on the evolution of metamorphic stars and their pollution rate at various radius in AGN disks. These results underline the importance of internal mixing for AGN-embedded stellar evolution and motivate future work on disk enrichment and stellar demographics.

Acknowledgements I thank Yi-Xian Chen, Douglas N. C. Lin, Mohamad Ali-Dib, and Timothy D. Brandt for helpful discussions. I am also grateful to the anonymous referee for constructive feedback that improved this manuscript. Discussions during the 2025 MESA Summer School in Leuven were especially valuable and are gratefully acknowledged.

References

Ali-Dib, M., & Lin, D. N. C. 2023, MNRAS, 526, 5824 2, 6, 7, 10

Artymowicz, P., Lin, D. N. C., & Wampler, E. J. 1993, ApJ, 409, 592 1

Cantiello, M., Jermyn, A. S., & Lin, D. N. C. 2021, ApJ, 910, 94 2, 5

Chen, Y.-X., Jiang, Y.-F., & Goodman, J. 2025, arXiv e-prints, arXiv:2505.13951 4

Chen, Y.-X., Jiang, Y.-F., Goodman, J., & Lin, D. N. C. 2024, ApJ, 974, 106 5, 7

Chen, Y.-X., Jiang, Y.-F., Goodman, J., & Ostriker, E. C. 2023, ApJ, 948, 120 10

Chen, Y.-X., & Lin, D. N. C. 2023, Mon. Not. Roy. Astron. Soc., 522, 319 10

Chen, Y.-X., & Lin, D. N. C. 2024, ApJ, 967, 88 2, 7, 10

Dittmann, A. J., Cantiello, M., & Jermyn, A. S. 2021, ApJ, 916, 48 2

Fryer, C. L., Huang, J., Ali-Dib, M., et al. 2025, MNRAS, 537, 1556 2, 6, 8, 10

Goodman, J., & Tan, J. C. 2004, ApJ, 608, 108 1

Graham, M. J., Ford, K. E. S., McKernan, B., et al. 2020, Phys. Rev. Lett., 124, 251102 2

Hamann, F., & Ferland, G. 1999, ARA&A, 37, 487 2

Hamann, F., Korista, K. T., Ferland, G. J., Warner, C., & Baldwin, J. 2002, ApJ, 564, 592 2

Heger, A., Langer, N., & Woosley, S. E. 2000, ApJ, 528, 368 2

Huang, J., Lin, D. N. C., & Shields, G. 2023, MNRAS, 525, 5702 2, 7

Jermyn, A. S., Dittmann, A. J., McKernan, B., Ford, K. E. S., & Cantiello, M. 2022, ApJ, 929, 133 2

Jermyn, A. S., Bauer, E. B., Schwab, J., et al. 2023, ApJS, 265, 15 5

Jiang, Y.-F., & Goodman, J. 2011, ApJ, 730, 45 1

Joyce, M., & Tayar, J. 2023, Galaxies, 11, 75 5

Kippenhahn, R., & Weigert, A. 1994, Stellar Structure and Evolution 2, 3

Langer, N., El Eid, M. F., & Fricke, K. J. 1985, A&A, 145, 179 3

MacLeod, M., & Lin, D. N. C. 2020, ApJ, 889, 94 1

Maeder, A., & Meynet, G. 2010, New Astron. Rev., 54, 32 4

Maeder, A., & Zahn, J.-P. 1998, A&A, 334, 1000 3

Mombarg, J. S. G., Rieutord, M., & Espinosa Lara, F. 2024, A&A, 683, A94 10

Nagao, T., Maiolino, R., & Marconi, A. 2006, A&A, 459, 85 2, 7

Paxton, B., Bildsten, L., Dotter, A., et al. 2011, ApJS, 192, 3 5

Paxton, B., Cantiello, M., Arras, P., et al. 2013, ApJS, 208, 4 5

Paxton, B., Marchant, P., Schwab, J., et al. 2015, ApJS, 220, 15 5

Paxton, B., Schwab, J., Bauer, E. B., et al. 2018, ApJS, 234, 34 5

Paxton, B., Smolec, R., Schwab, J., et al. 2019, ApJS, 243, 10 5

Pedersen, M. G., Aerts, C., Pápics, P. I., et al. 2021, Nature Astronomy, 5, 715 3

Prat, V., & Lignières, F. 2014, Astronomy Astrophysics, 566, A110 4

Shankar, F., Weinberg, D. H., & Miralda-Escudé, J. 2009, ApJ, 690, 20 10

Sirko, E., & Goodman, J. 2003, MNRAS, 341, 501 1

Spruit, H. C. 2002, A&A, 381, 923 3, 4

Tagawa, H., Haiman, Z., & Kocsis, B. 2020, ApJ, 898, 25 2

Wang, S., Jiang, L., Shen, Y., et al. 2022, ApJ, 925, 121 2, 7

Yu, Q., & Tremaine, S. 2002, MNRAS, 335, 965 10

Zahn, J. P. 1992, A&A, 265, 115 3